Hindawi
Advances in Materials Science and Engineering
Volume 2019, Article ID 3635974, 16 pages
https://doi.org/10.1155/2019/3635974

Research Article

An Experimental Study of the Impact Mechanical Properties of RC Beams following Replacements of Stainless Steel Reinforcements of Equal Strength

Xiwu Zhou,[1] Runcheng Zhang,[1] Ruisheng Xiong,[2] Guoxue Zhang,[1] and Xiangyu Wang[1]

[1]*Foshan University, Department of Civil Engineering, Guangdong, Foshan 528000, China*
[2]*Xinyang Normal University, Department of Civil Engineering, Henan, Xinyang 464000, China*

Correspondence should be addressed to Runcheng Zhang; 13006756502@163.com

Received 12 January 2019; Accepted 30 April 2019; Published 3 June 2019

Academic Editor: Tomasz Trzepieciński

The reinforced concrete structure of a port wharf is affected by steel corrosion and ship docking impact. Replacing an ordinary steel bar with a stainless steel bar can solve the corrosion problem of the steel bar while ensuring the bearing capacity of the structure. However, the research on impact resistance of stainless steel-reinforced concrete structure is not perfect. In this paper, impact mechanical properties of reinforced concrete beams before and after equal strength replacement of stainless steel bars are analyzed by theoretical analysis and drop hammer impact test, and the possibility and applicable scope of equal strength replacement of stainless steel bars are put forward. The results indicated the following: (1) when the reinforcement ratios were small (0.21% to 1.32%), the stainless steel-reinforced concrete beams with equal strength were able to effectively reduce the stiffness losses of the beams undergoing impact loads, as well as improve the elastic resilience abilities, and reduce the structural damages. Therefore, the corrosion and impact problems of reinforcements could be solved by replacing ordinary reinforcements with stainless steel reinforcements and (2) when the reinforcement ratios were large (1.32% to 2.57%), the shear failures of the stainless steel-reinforced concrete beams were observed to be relatively serious, and the impact resistance performances had worsened. The research results provide technical support for the engineering application of stainless steel-reinforced concrete structure design.

1. Introduction

In coastal areas, such as buildings and marine engineering, where reinforcement corrosion is prone to occur, people begin to use stainless steel bars [1] instead of ordinary steel bars to solve the problem of steel bar corrosion. However, these structures are likely to be subjected to impact loads. Under impact loading, the dynamic mechanical properties of reinforced concrete structures are very complicated due to the nonlinearity, geometric nonlinearity, and contact nonlinearity of steel and concrete materials. The impact mechanical properties of stainless steel-reinforced concrete structures are different from those of ordinary reinforced concrete structures. The impact mechanical properties of ordinary reinforced concrete structures and the static load mechanical properties of stainless steel-reinforced concrete structures have been studied by many scholars. However, the impact mechanical properties of stainless steel-reinforced concrete structures are less studied.

Previously, researchers have carried out static load tests on stainless steel-reinforced beams. For example, Zhang et al. [2] conducted an experimental study on the mechanical properties of stainless steel-reinforced concrete beams. The results showed that the ultimate bearing capacities of the examined stainless steel-reinforced concrete beams had been improved when compared with that of ordinary reinforced concrete beams. However, the amplitudes of increases were small. Meanwhile, the deflection values of the beams had been increased to a large extent. Zhang et al. [3] also carried out quasi-static tests on stainless steel-reinforced concrete beams. The results indicated that, when compared with the ordinary reinforced concrete beams, the yield displacements,

ultimate displacements, and displacement ductility coefficients of the stainless steel-reinforced concrete beams had been significantly increased. Furthermore, the ductility performances were improved, and the strength and stiffness degradations were relatively gentle, which indicated good seismic performances. Li et al. [4] compared the bending bearing capacities and shear bearing capacities of stainless steel-reinforced concrete beams with those of ordinary reinforced concrete beams. After the results were analyzed, it was concluded that there were no significant differences between the stainless steel-reinforced concrete beams and the ordinary reinforced concrete beams in terms of the actual measured values and the theoretical values of the cracking moments and ultimate bending moments. However, the actual measured ultimate shear values of the stainless steel-reinforced concrete beams were observed to be significantly higher than those of the ordinary reinforced concrete beams. Previously, studies regarding the performances of reinforced concrete beams undergoing impact loads have been carried out by both Chinese and international researchers. For example, Hughes and AI-Dafiry [5] studied the mechanism of impact energy dissipation in different beam parts using drop weight test processes on reinforced concrete beams. Also, Kishi et al. [6] carried out drop weight experimental tests on eight beams with web reinforcements. The results showed that the maximum reaction force which occurred at the point of the beam failure could be used to estimate the ultimate strength of the bending failure-type reinforced concrete beams subjected to impact loading. In another related study, Bentur et al. [7] measured the accelerations of the measured points of beams in experimental drop weight tests. The measurement results indicated that the accelerations of the beams were very large during the initial stages of the impacts, and the impact forces were mainly resisted by the inertia force during the first stages. In the experiments conducted by Fujikake et al. [8], it was found that the ratios of the longitudinal reinforcements had affected the failure modes of the beams under the impact load conditions. Saatci and Vecchio [9] carried out drop weight impact tests on reinforced concrete beams with hammer heads of different masses and found that the bearable impact forces of the beams had increased with the increases in the shear strength. Pham et al. [10] found through experimental research that the local failures of the RC beams at the impacted locations had formed plastic hinges, and the propagation along the axis had potentially affected the impact resistance performances of the RC beams. Fu and Dong [11] carried out the test of drop hammer impact on reinforced concrete beams and discussed the failure mechanism of reinforced concrete structures under different impact height conditions. Zhan et al. [12] carried out drop weight tests on reinforced concrete beams and analyzed the influences of different impact velocities on the maximum bearing capacities and deformations of RC beams. Shen [13] examined the effects of the reinforcement ratios on the fracture behaviors of reinforced concrete beams, as well as the crack limiting effects of the reinforcements during crack propagation processes. However, at the present time, there have been few experimental studies regarding the performances of stainless steel RC beams under impact loading conditions.

Drop weight testing processes are effective methods which are used to study the damages incurred by reinforced concrete beams under impact load conditions. In this study, impact tests were carried out for three groups of reinforced concrete beams using a domestically advanced ultrahigh heavy drop hammer impact test machine system. The impact resistance performance results and failure modes of ordinary reinforced concrete beams and those with stainless steel replaced reinforcements of equal strength were compared in this study. It is used to evaluate the possibility of replacing ordinary steel bar with stainless steel bar and put forward its applicable scope to guide practical engineering application.

2. Overview of the Experimental Processes

2.1. Designs of the Beam Specimens. The beam specimens which were used in this experiment were 2,000 mm in length and had a span of 1,800 mm. The sectional dimensions were $b \times h = 150\ mm \times 300\ mm$, and the protection layer thickness was 25 mm. The layout of the reinforcements is shown in Figure 1, in which the L20 specimen beam was taken as the example.

According to the code requirements, in order to avoid the occurrence of cable-stayed damage and baroclinic damage, the stirrups used for the beam specimens were unified as Grade I ordinary steel reinforcements HPB300 with a diameter of 8 mm. The spacing of stirrups is 150 cm. The erection reinforcements were unified as two Grade III ordinary steel reinforcements HRB400 with a diameter of 10 mm. The bottom reinforcements were made partly of Grade III ordinary steel bar HRB400 and also made partly of S2304 duplex stainless steel reinforcements (UGIGRIP1. 4362), which had been produced by UGITECH Co. (France). The mechanical properties of steel bars measured by the tensile test of reinforcing bars with an universal tester, in which the stress value of the stainless steel reinforcements when the residual deformation was 0.2% was taken as the yield strength, as shown in Table 1. The C40 concrete which was utilized in this study's experimental testing processes was provided by a local commercial concrete company, and its mix proportion is shown in Table 2. According to the requirements of the code, the maximum particle diameter of coarse aggregate for concrete shall not be greater than 1/4 of the minimum size of structural cross section and 3/4 of the minimum net distance between reinforcement bars. In total, 12 cubic specimens ($150\,mm \times 150\,mm \times 150\,mm$) were made at the same time during the concrete placement of the components. The material strength was tested using a universal testing machine (WAW-2000), and the test results are shown in Table 3.

In order to compare and analyze the impact resistance of reinforced concrete beams before and after equal strength replacement of stainless steel bars, three groups of (total of 6 pieces) of reinforced concrete beams were designed according to the incremental sequences of the reinforcement ratios, as shown in Table 4. For example, Group A had a relatively small reinforcement ratio, and bending failure was this group's

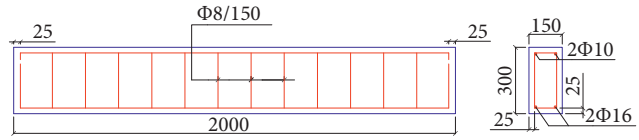

Figure 1: Layout of the reinforcements of the L20 specimen beam (mm).

Table 1: Properties of the reinforcement material.

Type of reinforcement	Diameters of the reinforcement	Modulus of elasticity (N/mm^2)	Yield strength (N/mm^2)	Ultimate strength (N/mm^2)	Yield bearing capacity (N)	Maximum bearing capacity (N)
HPB300	8	2.10×10^5	300	420	15079.64	21111.50
S2304	12	1.95×10^5	990	1165	111966.36	131758.39
	16		850	1000	170902.64	263893.78
	20		840	988	263893.78	310389.35
HRB400	18	2.00×10^5	420	620	106876.98	157770.78
	20		530	650	166504.41	204203.52
	25		530	650	260163.14	319068.00

Table 2: C40 Concrete mix ratio kg/m^3.

	Cement	Sand	Pebble	Water	Admixture	Additive
C40	293	674	1053	185	195	3.90
Remarks	Strength level: 42.5 MPa	Fineness modulus: 2.8 Density: 2640 kg/m^3	Particle size: 5~25 mm Density: 2730 kg/m^3	—	Blast furnace slag	FN-200 water reducing agent

Table 3: Mechanical properties of the concrete.

	Standard value of the compressive strength (MPa)	Modulus of elasticity (MPa)
C40 concrete	45.30	3.25×10^4

main failure mode under static concentrated load conditions. Group B had a moderate reinforcement ratio and bending and shearing failures were the main failure modes for this group under static concentrated load conditions. Finally, Group C had a relatively large reinforcement ratio, and shearing failure was determined to be the main failure mode under static concentrated load conditions for this group.

As can be seen in Table 4, the bearing capacities of the beams which had been subjected to vertically concentrated loads had changed after the approximately equal strength replacements of stainless steel reinforcements had taken place in the three groups. However, since the relative ratio was small, it was considered that the replacements had little effect on the bearing capacities of the members.

2.2. Experimental Devices and Data Collection. The loading device which was used in this study's experiment was an ultrahigh heavy drop hammer impact test machine, as detailed in Figure 2. The beams were placed on fixed hinge supports, and the drop hammer impacted the beams along the vertical guide rail with an approximated free fall motion. The mass of the drop hammer could be adjusted using a counterweight steel plate. The drop hammer head was a cylindrical flat hammer head with a diameter of 200 mm. A force sensor was built into the hammer head for the purpose of measuring the impact forces, as illustrated in Figure 3. The impact velocities of the drop hammer were measured using a laser velocimeter which had been placed above the beams in order to directly measure the instantaneous velocity before the hammer head had contacted the beams. During the experiment, the instantaneous velocity before the hammer contacts the beam is measured directly by the time required to change the signal of the laser probe through a small length of reflector and the length of the reflector through the laser trigger, as shown in Figure 4. At the bottom of the beam, a KTC-300 rod-type displacement meter is arranged to measure the midspan deflection with a measuring range of 300 mm and a precision of $300\pm0.05\%$, as shown in Figure 5. Finally, an AOS X-MOTION high-speed camera (produced by the Swiss AOS Technologies AG Co.) was used to record the processes of the impact tests, as shown in Figure 6.

In this experimental study, in order to analyze the deformations of the tensioned reinforcements in the beams under impact conditions, a resistance strain gauge was used to measure the strain of the reinforcements. The distribution of the measuring points is shown in Figure 7. The strain gauge which was utilized in this study's test processes was produced by the Zhejiang Huangyan Testing Apparatus Factory. Also, the type of steel strain gauge used in the tests was BX120-3AA, which had a grid length of 3×2 mm, a resistance value of $119.9\pm0.1\ \Omega$, and a sensitivity coefficient

Table 4: Design parameters of the specimens.

Group	Specimen	Diameter of bottom reinforcement (mm)	Reinforcement ratio (%)	Shear bearing capacity (kN)		Bending bearing capacity (kN·m)	
				Yielding	Ultimate	Yielding	Ultimate
A	L18	18	1.32	80.76	113.06	51.97	76.72
	S12	12	0.58	80.76	113.06	53.70	63.19
B	L20	20	1.63	80.76	113.06	78.03	95.70
	S16	16	1.04	80.76	113.06	79.63	93.68
C	L25	25	2.57	80.76	113.06	115.56	141.72
	S20	20	1.63	80.76	113.06	116.07	136.52

S represents the stainless steel reinforcement (S2304).

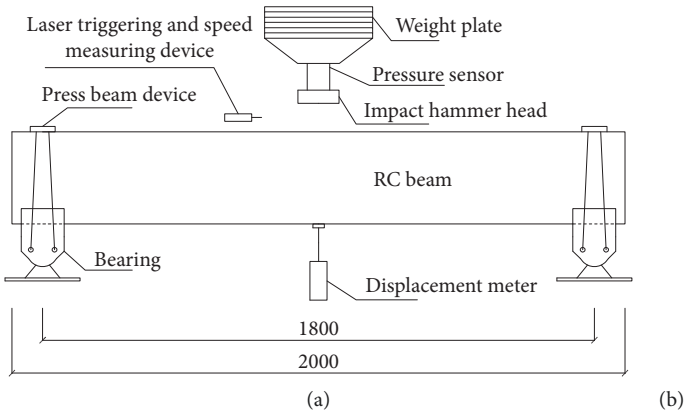

Figure 2: Drop hammer impact test device (mm).

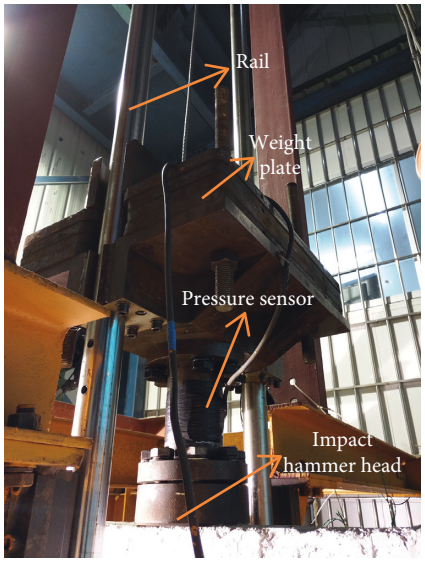

Figure 3: Drop hammer.

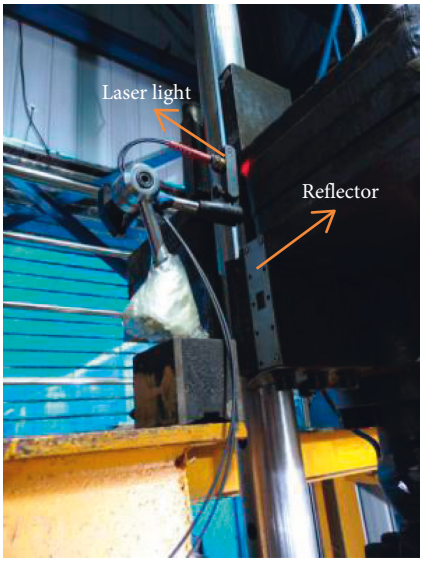

Figure 4: Laser trigger and velocity measuring device.

of 2.06 + 1%. The concrete strain gauge which was adopted in this study's experiment was a BX120-80AA type, which had a grid length of 80 × 3 mm, a resistance value of 119.9 ± 0.1 Ω, and a sensitivity coefficient of 2.06 + 1%. The cracks in the beams which had occurred after each test were measured using a crack width gauge. The data acquisition system used in this study's tests was NIPXIe-1006Q, which had been produced by the National Instruments Co. Ltd. As can be seen in Figure 8, all of the data signals obtained from the various devices, such as the resistance strain gauge, pull rod-type displacement gauge, and pressure sensor, were voltage signals during the tests. These were collected into LabVIEW SignalExpress graphic interactive software using the aforementioned NIPXIe-1006Q dynamic acquisition

Figure 5: Displacement gauge.

Figure 6: High-speed camera.

instrument. A KD5005 charge amplifier was used for this study's postprocessing. The data acquisition frequency was set as 1 MHz.

2.3. Designs of the Experimental Processes. In the current study, a drop hammer was lifted to a certain height along a track by a fixture, and the fixture was loosened in order to cause the drop hammer to move along the track in an approximated free-fall motion. Then, the drop hammer had acted directly on the top surfaces of the midspan areas of the beam specimens. The drop hammer mass which was used in this experiment was 400 kg, and the drop hammer was raised to the heights of 0.5 m, 1.0 m, and 1.5 m in turn. Three impact tests were carried out on each beam specimen. The track friction had been successfully measured as 1,895 N, 1356.72 N, and 1,195.95 N, respectively. The theoretical

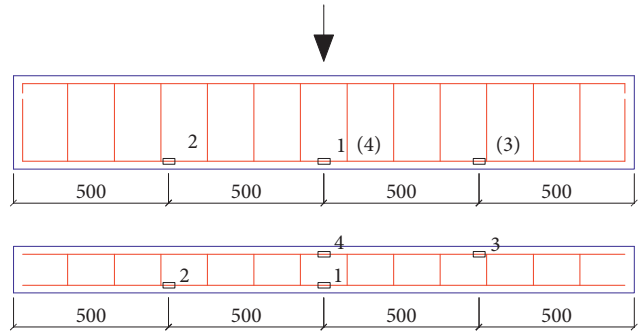

Figure 7: Distribution of the steel strain gauge.

Figure 8: Data collection system.

impact velocities were 2.25 m/s, 3.58 m/s, and 4.52 m/s according to the kinetic energy theorem. During each of the impact tests, the impact velocities and impact forces of the drop hammer, along with the midspan displacements, strain levels of the reinforcements and concrete at the measuring points, and crack propagation of the specimens during the impacts, were collected and recorded.

3. Experimental Results and Analysis

By comparing and analyzing the impact forces, midspan displacements, steel strain levels at the measuring points, and the crack propagations of the three groups of beams under the same impact energy conditions, the impact resistance performances of both the ordinary reinforced concrete beams and the stainless steel-reinforced concrete beams after equal strength replacements were examined and compared in the present study.

3.1. Time History Curves of the Impact Forces. The time history curves for impact forces of the three groups of beams

during each of the impact processes are shown in Figure 9. In the current study, for the convenience of comparison, the starting time of each impact was set to 0 : 00.

As can be seen in Figure 9, the impact force time history curves of the ordinary reinforced beams and stainless steel-reinforced beams had displayed consistent changing trend during each impact. That is to say, the drop hammer had collided with the beams and had then undergone postpeak oscillations which tended toward the horizontal. The durations of the subsequent wave crest formations were observed to be approximately the same (approximately 1 ms).

During this study's experimental processes, in order to facilitate a comparison of the peak impact forces, the peak impact force-velocity curves of each group of beams were plotted, as shown in Figure 10.

As shown in Figure 10, the peak impact forces had increased with the increases in the impact energy for each of the beam specimens. For example, in regard to Group A, the peak impact forces of the two beams were observed to be similar to each other at the first impact, with a difference of 10.75%. This was determined to be due to the fact that before the beams had become damaged, the concrete had played a major role and the participation of the steel bars was not high. However, during the second and third impacts, the concrete had undergone cracking, and the reinforced bars had played a major role. During the second and third impacts, the peak impact forces of the S12 beam were 16.70% and 23.64% higher than those of the L18 beam, respectively, which indicated that the overall stiffness of the S12 beam was relatively large.

For Group B, the differences in the peak impact forces between the ordinary reinforced concrete beams and the stainless steel-reinforced concrete beams following the equal strength replacements were found to be less than 5%. These results indicated that the equal strength replacements of the stainless steel reinforcements had less influence on the overall stiffnesses of the beams.

For Group C, the peak impact forces of the two beams were observed to be similar at the first impact. The peak impact forces of the L25 beam were 5.83% and 18.10% higher than those of the S20 beam at the second and third impact, respectively. These results showed that with the increases in the impact velocities, the stiffness losses of the stainless steel-reinforced concrete beams of equal strength replacements had been faster.

In summary, the impact forces were found to be mainly related to the concrete when the first impacts had occurred. At those stages, the participation of the steel bars had not been high, and the impact forces of the ordinary steel beams and stainless steel-reinforced beams of equal strength replacements were determined to be similar. However, during the second and third impacts, cracks had occurred in the beam concrete, and the tensioned reinforcements had played major roles. At that time, the impact forces were related to the tensioned reinforcements. It was observed that when the reinforcement ratios were small (0.21% to 1.32%), the stainless steel-reinforced beams of equal strength replacements had larger peak impact forces, and the overall stiffness losses of the beams had been slower. However, when the reinforcement ratios were high (1.32% to 2.57%), the differences in the peak impact forces between the stainless steel-reinforced beams of equal strength replacements and the ordinary steel beams had gradually decreased. Furthermore, the peak impact forces of the stainless steel-reinforced beams of equal strength replacements had become even lower than those of the ordinary steel beams, which was determined to be related to the failure modes.

3.2. Time History Curves of the Displacements. During this study's experimental testing, the midspan deflections of the beams were measured using a displacement meter located at the bottom of the midspan. The displacement time history curves of the three groups of beams during each impact are detailed in Figure 11.

As detailed in Figure 11, the change trends of the displacement time history curves of the ordinary steel bar beams and stainless steel-reinforced beams were consistent during each of the impacts. In other words, the drop hammer had collided with the beam; the midspan displacements had increased and then had dropped after reaching the peak values resulting in main wave crest formations. Then, the displacements had continued to decrease (some of which had reached negative values) and had risen again after reaching the minimum values, resulting in wave trough formations. It was observed that when the displacements had risen to a certain value, the curves had tended to be horizontal, characterized in part by residual deformations. The durations of the main wave crests were approximately 15 ms to 30 ms, which were much longer than the duration of 1 ms observed for the wave crests of the impact forces. These findings suggested that the overall deformations of the beams were just beginning after the impacts. At those times, the beams were in stages of overall responses, and the stress had been transferred along the entire lengths of the beams. Therefore, the impact energy had been consumed by the entire beams through deformations. The durations of the main peak crests were determined to be related to the impact energy. It was observed that for the same beam, the higher the impact energy was, the larger the displacement would be, and the longer the durations of the main wave peaks would be.

In regard to Group A, the peak durations of the displacement time history curves of beams L18 and S12 were observed to be similar. The residual deformations of the two beams after each impact had increased with the increases in the impact energy. The residual deformations of the stainless steel-reinforced S12 beam of equal strength replacements were determined to be 43.12% lower than those of the L18 beam. Therefore, the results indicated that replacement of ordinary steel reinforcements with stainless steel reinforcements of equal strength could effectively improve the elastic resilience of the beams, as well as reduce the residual deformations.

For Group B, the residual deformations of beam L20 were observed to gradually increase with the increases in the impact energy, which approximately ranged from 1 to 10 mm. It was found that for the S16 beam, the elastic

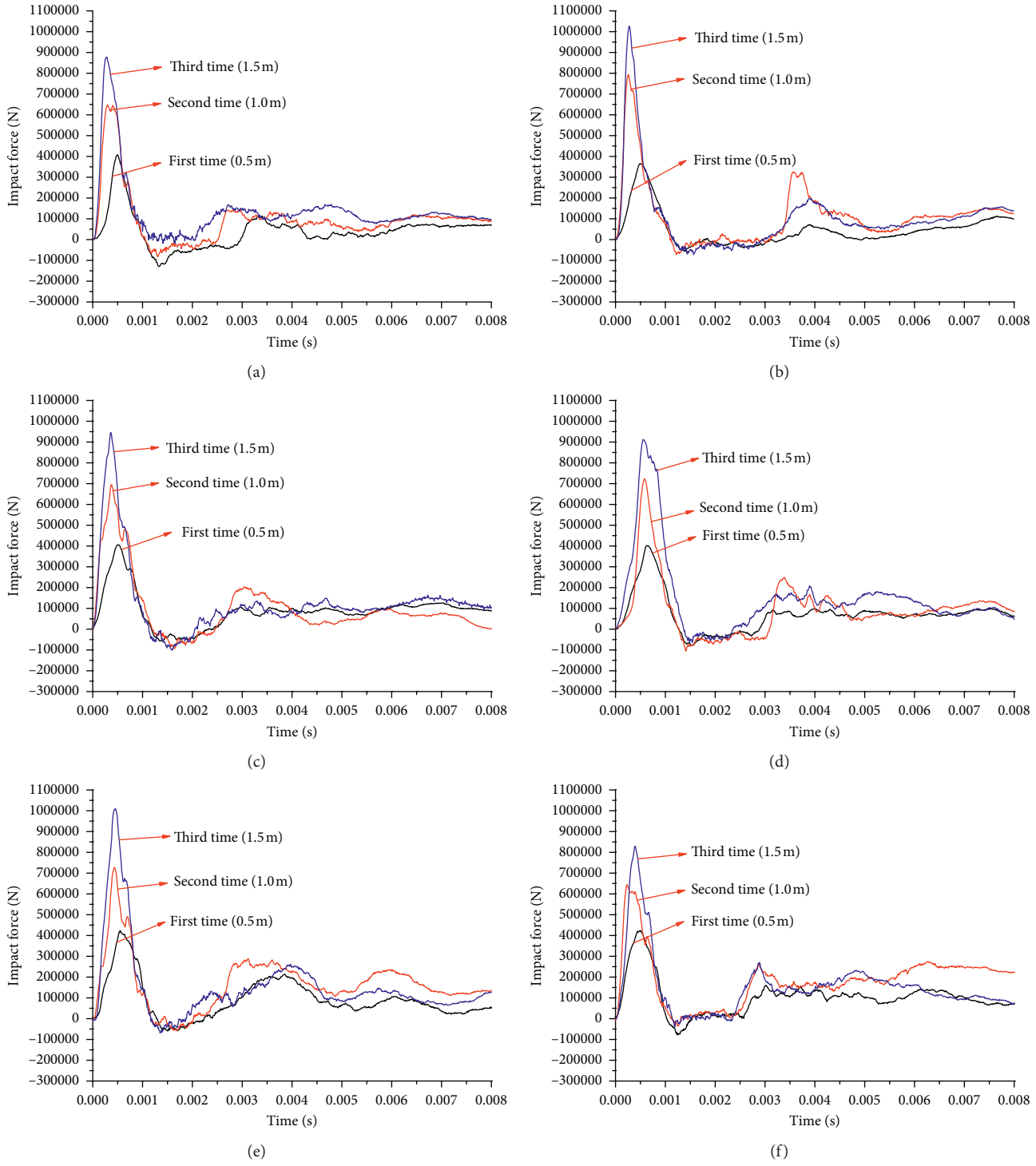

Figure 9: Time history curves of the impact forces. Group A: (a) L18 and (b) S12. Group B: (c) L20 and (d) S16. Group C: (e) L25 and (f) S20.

resilience abilities were better and the displacements had basically recovered after the first and second impacts. However, the residual deformations had suddenly increased after the third impact, which was approximately 33 mm.

It was observed that for Group C, the elastic resilience abilities of the L25 and S20 beams were better, and the displacements had basically been restored following the first and second impacts. However, after the third impact, the residual deformations of the L25 beam were observed to be approximately 7.5 mm, while those of the S20 beam had suddenly increased to 27.5 mm.

In conclusion, it was determined in this study that when the reinforcement ratios were small, the elastic resilience abilities of the beams could effectively be improved and the residual deformations could be reduced by replacing the ordinary reinforcements with stainless steel reinforcements

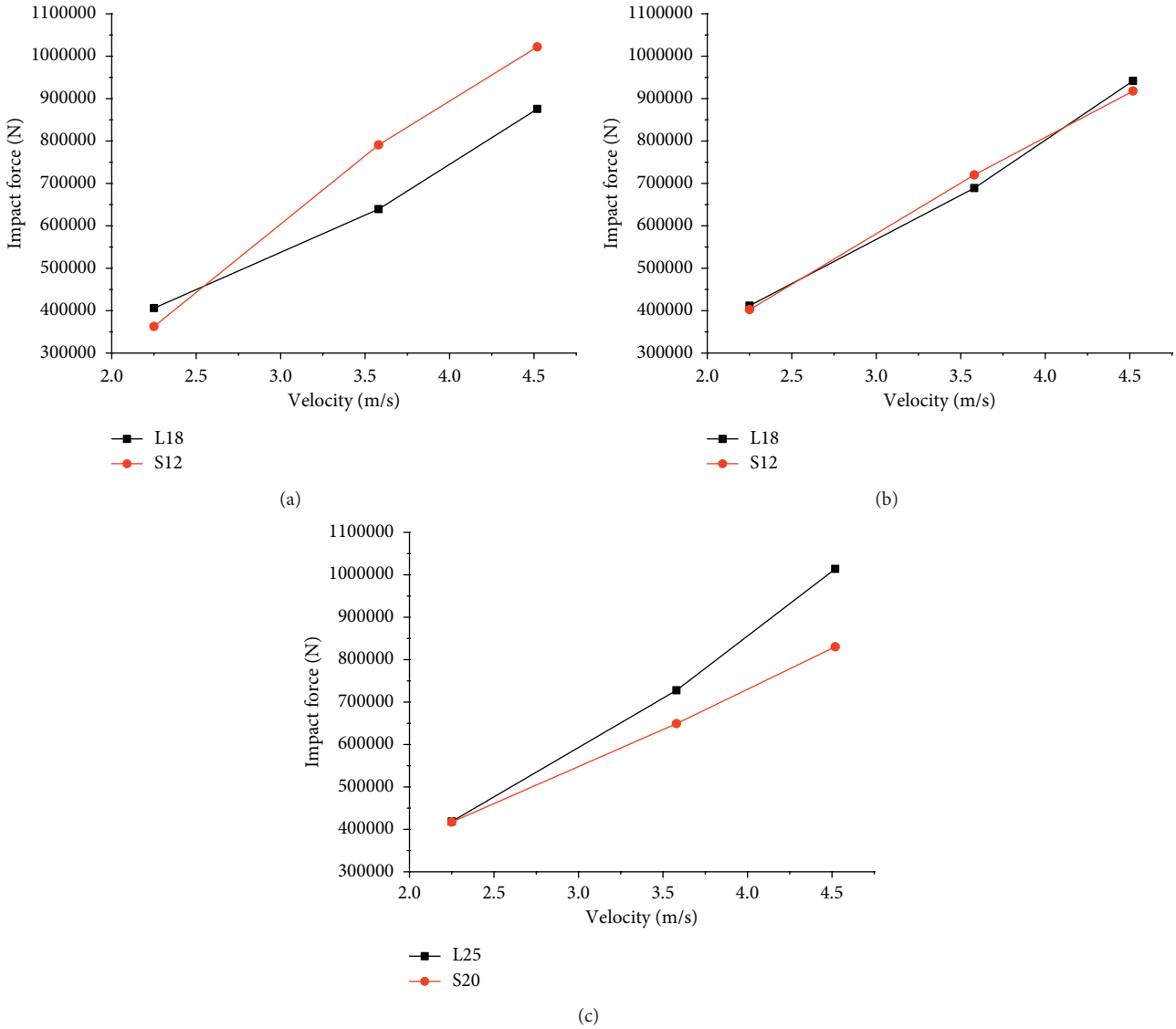

Figure 10: Peak impact forces and velocity curves. (a) Group A. (b) Group B. (c) Group C.

of equal strength. However, when the reinforcement ratios were high, it was found that while comparing the ordinary reinforced beams, the beams with reinforced stainless steel of equal strength replacements had brittle characteristics. It could be seen from the experimental results that when the impact energy was small, they had shown better elastic resilience abilities, and the residual deformations were approximately 0. However, when the impact energy had accumulated to a certain extent, the residual deformations had suddenly increased, and the elastic resilience abilities basically lost without warning.

In the current study, for the convenience of comparing the peak values of the displacements, the peak displacement-velocity curves of each group of beams were plotted, as shown in Figure 12.

As shown in Figure 12, the differences in the peak displacements between the two beams were relatively stable for Group A, and the average peak displacement of the S12 beam was determined to be 17.23% higher than that of the L18 beam. For Group B, the differences between the two beams had gradually increased with the increases in the impact velocities. The peak displacements of the S16 beam were 17.15%, 15.23%, and 35.35% higher than those of the L20 beam, respectively. In regard to Group C, it was found that the peak displacements of the S20 beam were 0.45%, 11.04%, and 20.43% higher than those of the L25 beam, respectively, which were similar to the results observed for Group B.

In summary, it was determined in this study that when the reinforcement ratios were small, the displacements of the stainless steel-reinforced beams after equal strength replacements were 17.23% higher than those of the ordinary reinforced concrete beams under the effects of different impact energies. Also, the displacement variation trends were found to be consistent. The elastic resilience capacities of the stainless steel-reinforced concrete beams were observed to be relatively large, and the residual deformations

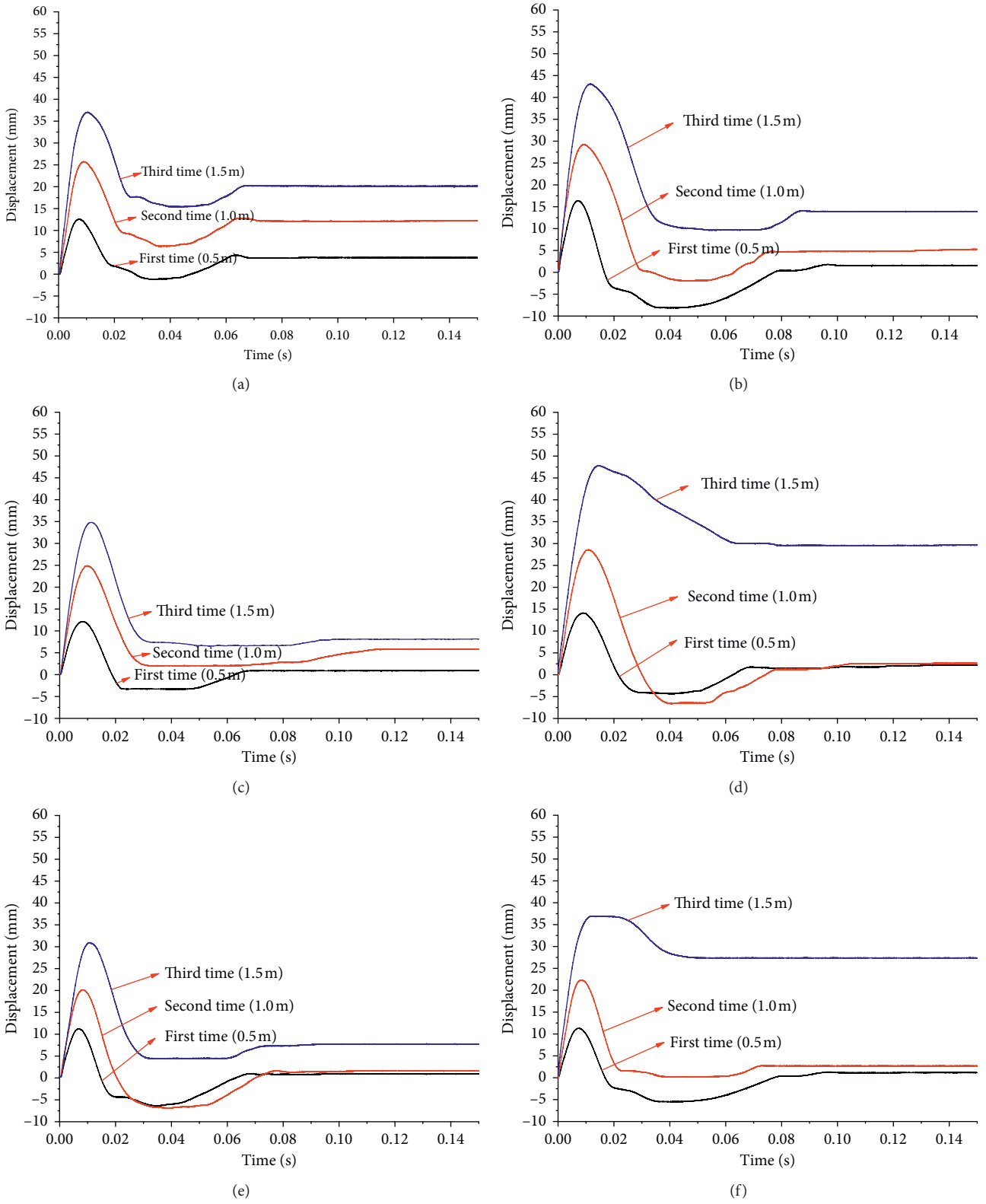

Figure 11: Time history curve of the displacements. Group A (a) L18 and (b) S12. Group B: (c) L20 and (d) S16. Group C: (e) L25 and (f) S20.

had been reduced by 43.12%. It was found that when the reinforcement ratios were high, the displacement peak values of stainless steel-reinforced beams after equal strength replacements were larger than those of the ordinary steel beams. This was determined to be due to the poor ductility of the stainless steel reinforcements. However, the

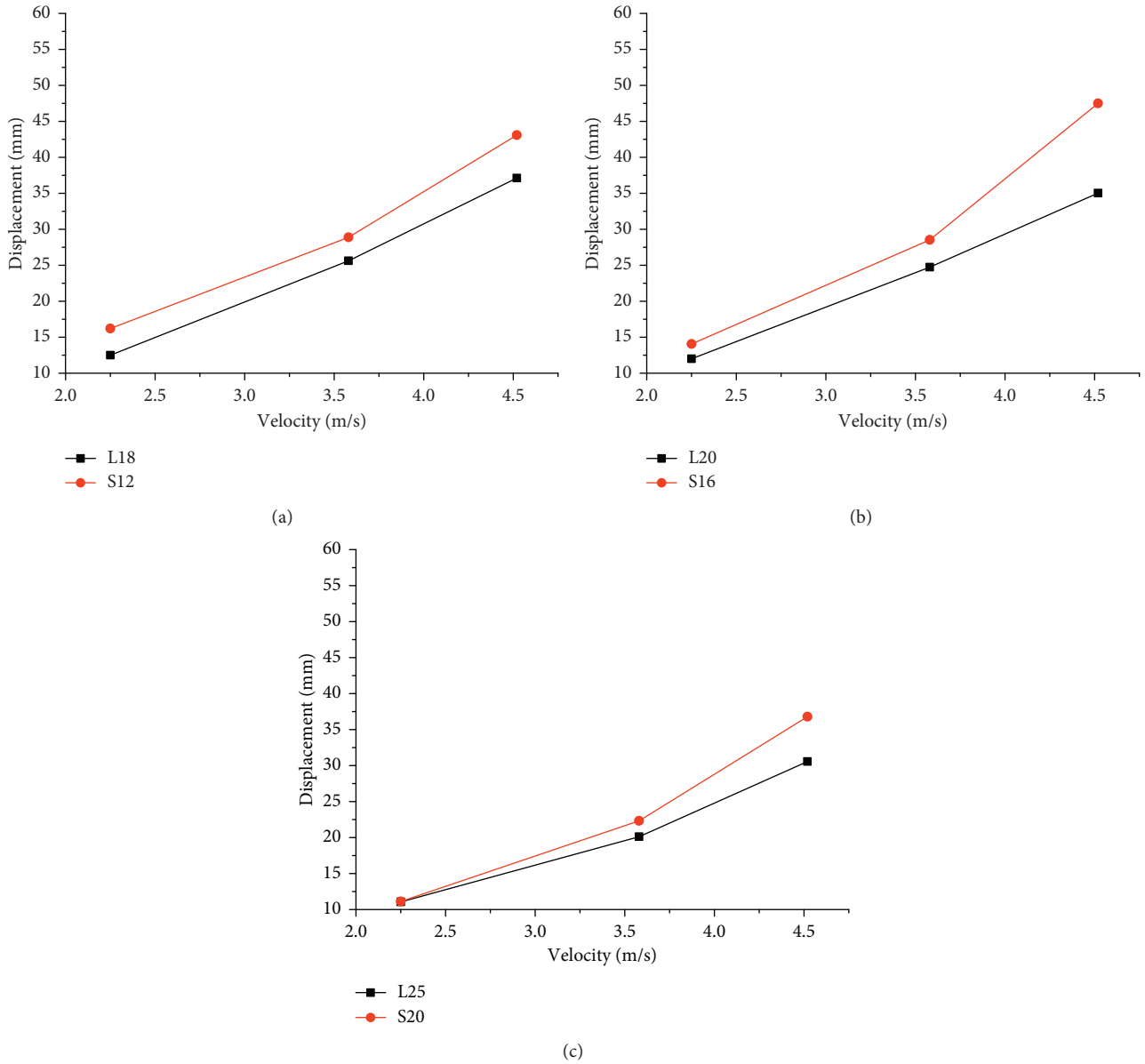

Figure 12: Peak displacements and velocity curves. (a) Group A. (b) Group B. (c) Group C.

displacement variation trends had significantly increased with the increase in the energy, which indicated that the shear failures of the beams were aggravated by the equal strength replacements when the reinforcement ratios were high.

3.3. Time History Curves of the Strain. During this study's experimental testing processes, the strain levels of the longitudinal reinforcements of the beams at the measuring points were obtained using a steel strain gauge. Due to the different failure modes of the beams and the different locations of the measuring points, it was found that the strain levels of the reinforcements had varied greatly. In the current study, the strain data ($\mu\varepsilon$) of the #3 reinforcement were selected for analysis purposes. The strain time history curves of the #3 reinforcement during each of the impact processes of the three groups of beams are shown in Figure 13.

As detailed in Figure 13, the steel strain time history curves of the ordinary and stainless steel-reinforced beams had displayed similar changing trends. That is to say, the drop hammer had collided with the beams. The steel strain had first increased and then decreased after reaching the peak values, resulting in main wave crest formations. At that point, the curves had tended to be horizontal. The steel strain time history curves were observed to be relatively simple. The durations of the main wave crests had ranged between 15 ms and 30 ms, which were found to be similar to the durations of main wave crests of the displacement time history curves.

In the current study, for the convenience of comparing the peak strains of the reinforcements, the peak strain-velocity curves of each group of beams were plotted, as illustrated in Figure 14.

As shown in Figure 14, for Group A, the peak strains of the L18 reinforcement were 69.93%, 11.85%, and 11.11%

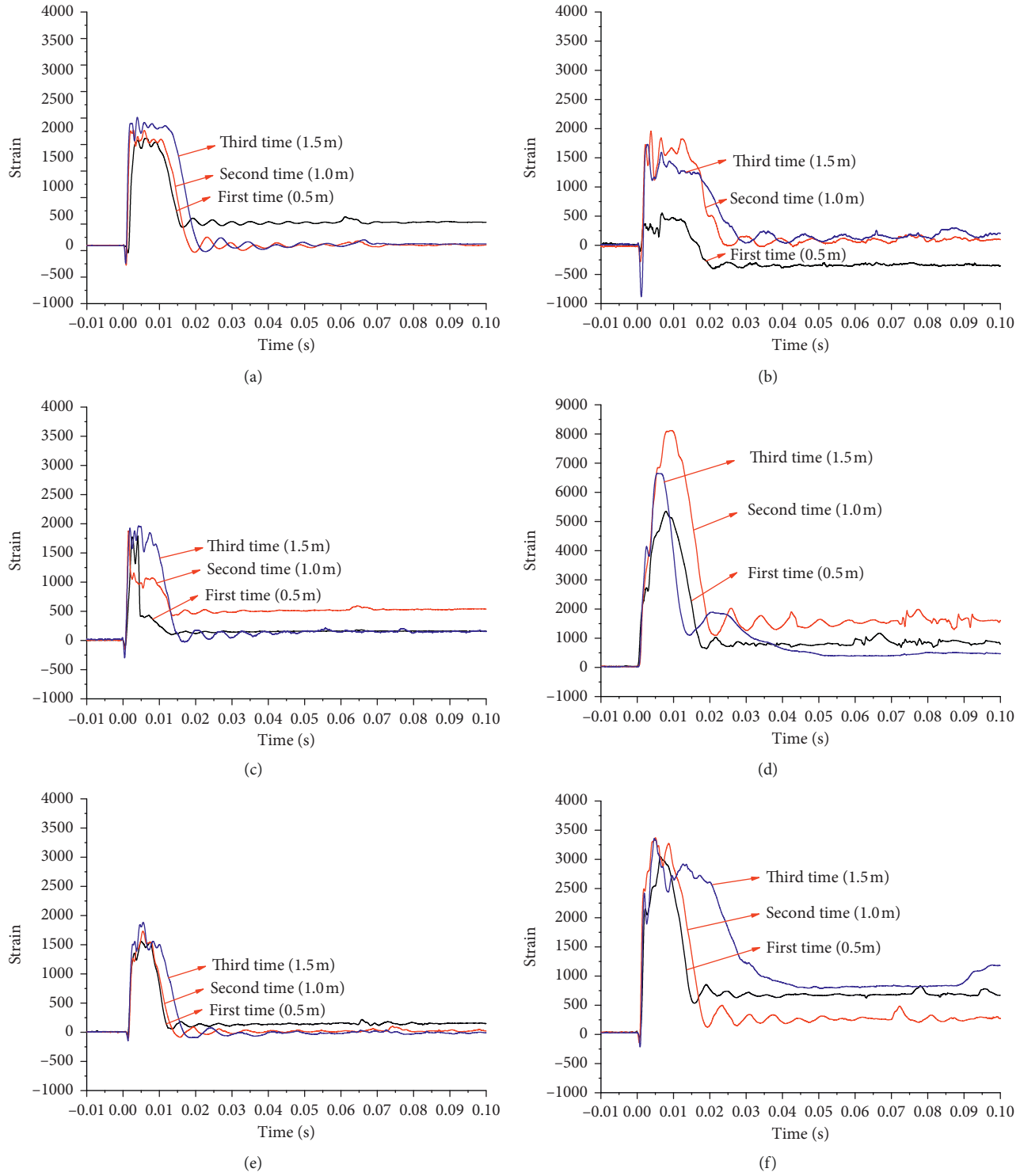

Figure 13: Time history curves of the steel strain. Group A: (a) L18-3# and (b) S12-3#. Group B: (c) L20-3# and (d) S16-3#. Group C: (e) L25-3# and (f) S20-3#.

higher than those of the S12 during the three impacts, respectively. Also, the strain levels of stainless steel reinforcements had obviously been reduced following the equal strength replacements. For Group B, the peak strains of the reinforcements in the S16 beam were observed to be much larger than those in the L16 beam, which may have been caused by the fact that the #3 measuring point situated at the shear failure location of the beam. For Group C, the peak strains of the reinforcement in the S20 beam during the three impacts were determined to be 96.67%, 96.26%, and 79.90% higher than those of the L25 beam, respectively. In summary, it was determined that the steel strain levels could

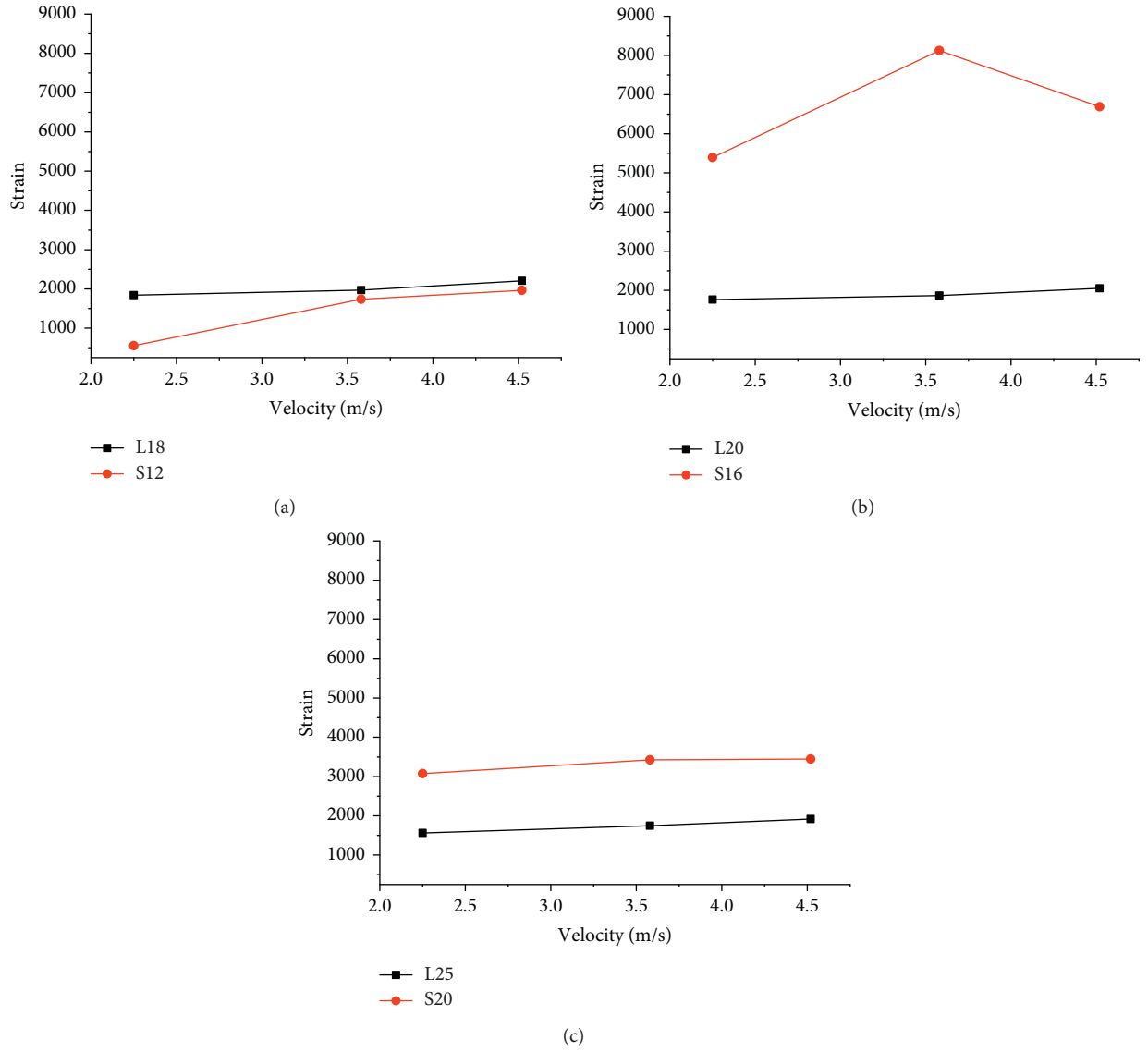

Figure 14: Strain peaks and velocity curves of each specimen group. (a) Group A. (b) Group B. (c) Group C.

be effectively reduced after the replacements with stainless steel reinforcements of equal strength when the reinforcement ratios were small. However, it was observed that the steel strain levels had increased after the replacements with stainless steel reinforcements of equal strength when the reinforcement ratios were large. It was concluded that this was mainly due to the fact that the replacements with stainless steel reinforcements of equal strength had a displaying trend of increasing shear failures of the RC beam.

3.4. Crack Propagations and Failure Modes. The crack propagations of the three groups of beams after each impact were recorded, as detailed in Table 5. The final failure pattern of the beam is shown in Figure 15.

By observing the crack development process and failure pattern of the beam, it is found that the cross section force of the beam under impact load is similar to that of the static load; that is, in the section subjected to bending moment, the upper part of the concrete is under compression and the lower part of the beam is under tension. When the bending moment increases to a certain extent, the concrete in the lower cross section is damaged by tension and the tensile force is borne by the reinforcement. Due to the large deformation of the tensile bar at the bottom, the neutralization axis moves upward and the compressive area of the concrete in the upper cross section decreases. The bending moment continues to increase until tensile steel bars yield or compressive concrete is destroyed. Because of the strain rate effect of concrete and reinforcement under impact load, the nonlinear deformation of beam cross section is more complex and whether it accords with the plane or not. The hypothesis of the cross section needs to be proved, and more precise measuring instruments are needed.

It was observed that for Group A, the cracks in the L18 beam had appeared in the midspan area at the beginning and had then propagated from bottom to top. The majority of those cracks were vertical cracks. It was found that with the

Table 5: Crack propagations.

Group number	Specimen number	Sketch for cracks (1st time to 3rd time)	Specimen number	Sketch for cracks (1st time to 3rd time)
A	L18	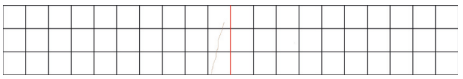 Number of cracks: 1 Maximum crack width: 0.32 mm 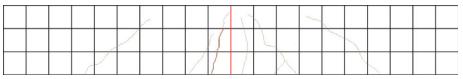 Number of cracks: 6 Maximum crack width: 1.72 mm 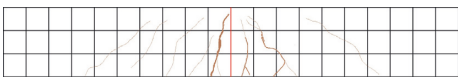 Number of cracks: 8 Maximum crack width: 2.46 mm	S12	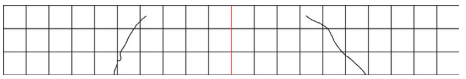 Number of cracks: 2 Maximum crack width: 0.14 mm 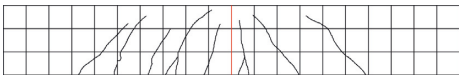 Number of cracks: 8 Maximum crack width: 0.60 mm 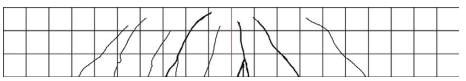 Number of cracks: 8 Maximum crack width: 2.20 mm
B	L20	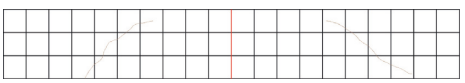 Number of cracks: 2 Maximum crack width: 0.77 mm 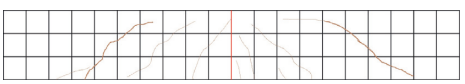 Number of cracks: 6 Maximum crack width: 0.87 mm 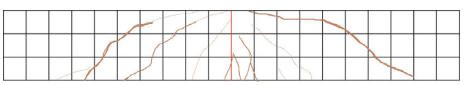 1 Number of cracks: 7 Maximum crack width: 1.92 mm	S16	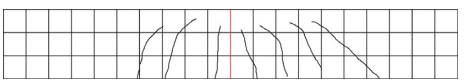 Number of cracks: 7 Maximum crack width: 0.15 mm 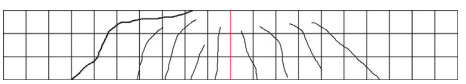 0 Number of cracks: 9 Maximum crack width: 1.26 mm 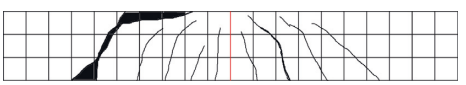 2 Number of cracks: 9 Maximum crack width: 20 mm
C	L25	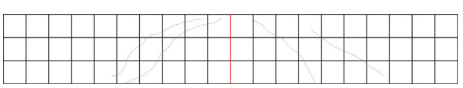 3 Number of cracks: 4 Maximum crack width: 0.16 mm 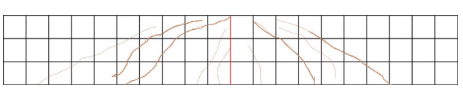 5 Number of cracks: 9 Maximum crack width: 1.00 mm 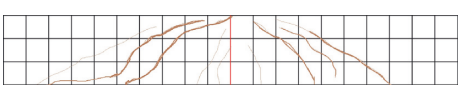 7 Number of cracks: 9 Maximum crack width: 3.56 mm	S20	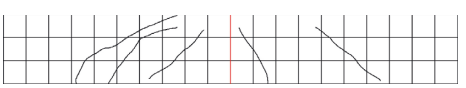 4 Number of cracks: 5 Maximum crack width: 0.13 mm 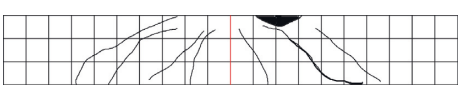 6 Number of cracks: 7 Maximum crack width: 2.66 mm 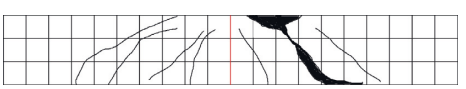 8 Number of cracks: 7 Maximum crack width: 22 mm

Figure 15: Beam failure form. (a) L18. (b) S12. (c) L20. (d) S16. (e) L25. (f) S20.

increases in the impact energy, the cracks in the midspan area had continued to expand and extend upward until they had penetrated the beam body. At the same time, multiple cracks at the bottom of the beam had extended to the top of the midspan area, and those cracks were observed to be evenly distributed. The cracks in the S12 beam had first appeared at 1/4 position of the beam body and had then propagated from the bottom to the top of the beam midspan area to form 45° oblique cracks. It was observed that with the increases in the impact energy, some smaller cracks had successively appeared in the beam midspan area and its vicinity. Also, a small number of cracks had propagated to

the top of the beam, and those cracks were found to be uniformly distributed, with only minor differences found in the widths of the cracks.

For Group B, the L20 beam cracks had appeared at the 1/4 position of the beam body at the beginning of the impact process and had propagated from the bottom to the top of the midspan area of the beam to form 45° oblique cracks. It was observed that with the increases in the impact energy, some small cracks had appeared in the midspan area of the beam and its vicinity. However, those cracks had propagated slowly, while the cracks at the 1/4 position of the beam body had propagated more quickly to become the main cracks. The cracks of the S16 beam had begun to distribute evenly from the midspan area of the beam to the 1/4 position location of the beam body and were mainly small oblique cracks. It was found that with the increases in the impact energy, the cracks near the midspan area of the beam had slowly propagated. Meanwhile, 60° oblique cracks had appeared at the 1/4 position location of the beam body and had rapidly propagated to become the main cracks. These cracks had subsequently penetrated the beam body, which then led to beam failure.

In regard to Group C, the crack propagation of the L25 beam was observed to be similar to that of the L20 beam. However, the cracks were found to be relatively narrow. The crack propagation of the S20 beam was determined to be similar to that of the S16 beam. The cracks began to be evenly distributed from the midspan area of the beam to the 1/4 location of the beam body and had the characteristics of small oblique cracks. It was found that with the increases in the impact energy, the cracks near the midspan area of the beam had propagated slowly and remained small. Meanwhile, 60° oblique cracks had occurred at the 2/3 position of the beam body and had rapidly propagated to become main cracks. Those cracked then penetrated the beam body, which subsequently led to beam failure.

In summary, for the L18 and S12 beams in Group A, bending failures were evident, and the crack propagation characteristics were observed to be similar. However, according to the number and widths of the cracks, the damage degree of the S12 beam was smaller, which indicated that stainless steel-reinforced concrete beams after equal strength replacements could effectively reduce beam damages and had displayed better impact resistance performances. For Group B, it was found that the L20 and S16 beams had mainly experienced shear failures. However, the main locations of the shear cracks were slightly different. It was determined that in accordance with the number and widths of the cracks, the damages to the S16 beam were less severe during the first impact. However, with the increases in the impact energy, the cracks had quickly propagated until the bearing capacity had been lost. It was determined that this was due to the fact that when the impact energy was larger, the strength of stainless steel reinforcements was higher; the deformations were smaller; and the energy absorption abilities were poor. Therefore, when the beams had impacted, the internal forces of the beams could not be released in time, and serious shear failures mainly occurred due to the concrete being subjected to impact forces. Therefore, the tensioned stainless steel of the S16 beam was found to not to be conducive for the components to bear the impact loads, and its overall impact resistance was poor. Generally speaking, it was found that the failure pattern of Group C was similar to that of Group B.

4. Conclusions

In the current research study, the data regarding the impact forces, midspan displacements, strains of the reinforcements at the measuring points, and the failure modes of three groups of stainless steel bars of equal strength replacing ordinary reinforced concrete beams under the same impact energy conditions were compared and analyzed. The following main conclusions were successfully achieved:

(1) The results revealed that during the local response stages, when the impact forces had incurred the dynamic responses of RC beam impacts, the sizes of the impact forces were mainly related to the overall stiffness of the RC beams, as well as the stiffness of the impact points. It was observed that when the reinforcement ratios were small, the replacements with stainless steel-reinforced concrete beams of equal strength were able to reduce the stiffness losses following cumulative impacts. This had also effectively improved the overall stiffnesses of beams, enhancing the impact resistance performances of the beams. However, when the reinforcement ratios were large, the stiffness losses were observed to be faster after the replacements with stainless steel-reinforced concrete beams of equal strength and the impact resistance abilities had become worse.

(2) It was found that for the maximum impact displacements of the RC beams, when the reinforcement ratios were small, the elastic resilience abilities of the beams could be improved by replacing the ordinary steel reinforcements with stainless steel bars of equal cross-sectional strength. However, when the reinforcement ratios were high, the brittle failure of the beams had been obviously increased under the impact loads due to the relatively small strain rate of stainless steel bars.

(3) In regard to the impact steel strain of the RC beams, it was found that when the reinforcement ratio was small, the replacements of the ordinary reinforcements with stainless steel reinforcements of equal cross-sectional strength could effectively reduce the strain levels of the tensioned reinforcements and improve the impact resistance performances of the beams. However, when the reinforcement ratios were large, the beams had displayed obvious brittle failures. Furthermore, the deformations had rapidly increased, and the impact resistance performances were observed to be poor.

(4) The failure modes of the beams were determined to be related to the deformation capacities and strength of the tensioned reinforcements. It was revealed in this study's results that when the reinforcement

ratios of the beams were small, the replacements of the stainless steel-reinforced piers with ordinary reinforcements had resulted in bending failures and good impact resistance performances. It was also found that when the reinforcement ratios of the beams were high, the shear failures were serious following the equal strength replacements.

In conclusion, the impact resistance performances of the beams examined in this study were found to be related to the ductility and strengths of the beams. It was observed that increased strength was able to enhance the bearing capacities of the beams, and better ductility had resulted in the beams absorbing more impact energy. Therefore, according to the characteristics of high strength and small deformations associated with the stainless steel reinforcements, it was concluded that when the reinforcement ratios of the beams were small (0.21% to 1.32%), the stainless steel bars of equal strength could be used to replace ordinary steel bars to solve the problem of steel corrosion. However, when the reinforcement ratios of the beams were high (1.32% to 2.57%), it was not recommended to use stainless steel reinforcements to replace ordinary reinforcements for reinforced concrete beams which may be subjected to impact loads.

Data Availability

The data used to support the findings of this study are available from the corresponding author upon request.

Conflicts of Interest

The authors declare that they have no conflicts of interest.

Acknowledgments

The authors would like to express their gratitude for the funding provided for this study from the Provincial-Level Major Scientific Research Projects of Guangdong Colleges and Universities (Grant no. 2014KZDXM064); as well as the funding provided by the Subject-Specific Funding Projects (Grant no. KJCX0188) of the Department of Education of Guangdong Province.

References

[1] H. Yuan, Y. Wang, and Y. Shi, "Preliminary study and application prospect of stainless steel reinforced concrete," *Building Science*, vol. 27, no. 5, pp. 101–105, 2011.

[2] G. Zhang, Y. Xu, and Z. Ding, "An experimental study of the flexural behaviors of stainless-steel reinforced concrete beams," *Railway Engineering*, vol. 407, no. 2, pp. 13–15, 2008.

[3] G. Zhang, F. Zhao, Z. Zhang, H. Zhang, X. Zhou, and D. Rao, "An experimental study of the seismic behaviors of stainless-steel reinforced concrete beams," *China Railway Science*, vol. 31, no. 5, pp. 35–40, 2010.

[4] C. Li, H. Geng, Q. Li, X. Zheng, and Y. Ou, "An experimental study of stainless-steel beams," *Journal of Highway and Transportation Research and Development (Applied Technology)*, vol. 13, no. 1, pp. 15–18, 2017.

[5] B. P. Hughes and H. AI-Dafiry, "Impact energy absorption at contact zone and supports of reinforced plain and fibrous concrete beams," *Construction and Building Materials*, vol. 9, no. 4, pp. 239–244, 1995.

[6] N. Kishi, O. Nakano, K. G. Matsuoka et al., "Experimental study on ultimate strength of flexural-failure-type RC beams under impact loading," in *Proceedings of the Transactions of 16th International Conference on Structural Mechanics in Reactor Techonology*, Washington, DC, USA, August 2001.

[7] A. Bentur, S. Mindess, and N. Banthia, "The behaviour of concrete under impact loading: experimental procedures and method of analysis," *Materials and Structures*, vol. 19, no. 5, pp. 371–378, 1986.

[8] K. Fujikake, B. Li, and S. Soeun, "Impact response of reinforced concrete beam and its analytical evaluation," *Journal of Structural Engineering*, vol. 135, no. 8, pp. 938–950, 2009.

[9] S. Saatci and F. J. Vecchio, "Effects of shear mechanisms on impact behavior of reinforced concrete beams," *ACI Structural Journal*, vol. 106, no. 1, pp. 78–86, 2009.

[10] T. Pham and H. Hao, "Prediction of the impact force on reinforced concreteiors of reinforced concrete deep beams undergoing impact effects," *Journal of Vibration and Shock*, vol. 34, no. 4, pp. 6–13, 2015.

[11] Q. Fu and X. Dong, "An experimental study of the responses and failures of reinforced concrete beams undergoing drop hammer impacts," *SCIENTIA SINICA Technologica*, vol. 46, no. 4, pp. 400–406, 2006.

[12] T. Zhan, Z. Wang, and J. Ning, "Failure behaviors of reinforced concrete beams subjected to high impact loading," *Engineering Failure Analysis*, vol. 56, pp. 233–243, 2015.

[13] P. Shen, "The effects of reinforcement ratios on the fracture parameters of concrete," *Journal of Disaster Prevention and Mitigation Engineering*, vol. 33, no. 2, pp. 235–240, 2013.